AGU PUBLICATIONS

Water Resources Research

RESEARCH ARTICLE

10.1002/2014WR015672

Probabilistic precipitation rate estimates with ground-based radar networks

Pierre-Emmanuel Kirstetter[1,2,3], Jonathan J. Gourley[2], Yang Hong[3], Jian Zhang[2], Saber Moazamigoodarzi[3], Carrie Langston[2,4], and Ami Arthur[2,4]

[1]Advanced Radar Research Center, University of Oklahoma, Norman, Oklahoma, USA, [2]NOAA/National Severe Storms Laboratory, Norman, Oklahoma, USA, [3]School of Civil Engineering and Environmental Sciences, University of Oklahoma, Norman, Oklahoma, USA, [4]Cooperative Institute for Mesoscale Meteorological Studies, University of Oklahoma, Norman, Oklahoma, USA

Key Points:
- Probabilistic radar QPE is derived at fine scale for precipitation types
- It is the basis for precipitation probability maps and precipitation ensembles
- It compares positively at the hourly time scale to the deterministic QPE

Correspondence to:
P.-E. Kirstetter,
pierre.kirstetter@noaa.gov

Citation:
Kirstetter, P.-E., J. J. Gourley, Y. Hong, J. Zhang, S. Moazamigoodarzi, C. Langston, and A. Arthur (2015), Probabilistic precipitation rate estimates with ground-based radar networks, *Water Resour. Res.*, *51*, 1422–1442, doi:10.1002/2014WR015672.

Received 4 APR 2014
Accepted 18 JAN 2015
Accepted article online 28 JAN 2015
Published online 9 MAR 2015

Abstract The uncertainty structure of radar quantitative precipitation estimation (QPE) is largely unknown at fine spatiotemporal scales near the radar measurement scale. By using the WSR-88D radar network and gauge data sets across the conterminous US, an investigation of this subject has been carried out within the framework of the NOAA/NSSL ground radar-based Multi-Radar Multi-Sensor (MRMS) QPE system. A new method is proposed and called PRORATE for probabilistic QPE using radar observations of rate and typology estimates. Probability distributions of precipitation rates are computed instead of deterministic values using a model quantifying the relation between radar reflectivity and the corresponding "true" precipitation. The model acknowledges the uncertainty arising from many factors operative at the radar measurement scale and from the correction algorithm. Ensembles of reflectivity-to-precipitation rate relationships accounting explicitly for precipitation typology were derived at a 5 min/1 km scale. This approach conditions probabilistic quantitative precipitation estimates (PQPE) on the precipitation rate and type. The model components were estimated on the basis of a 1 year long data sample over the CONUS. This PQPE model provides the basis for precipitation probability maps and the generation of radar precipitation ensembles. Maps of the precipitation exceedance probability for specific thresholds (e.g., precipitation return periods) are computed. Precipitation probability maps are accumulated to the hourly time scale and compare favorably to the deterministic QPE. As an essential property of precipitation, the impact of the temporal correlation on the hourly accumulation is examined. This approach to PQPE can readily apply to other systems including space-based passive and active sensor algorithms.

1. Introduction

For decades, precipitation estimated from remote-sensing systems has been widely evaluated for its impact on the energy budget and the hydrological cycle. They are becoming even more scrutinized due to the changing climate as well as new missions that have been launched such as the Global Precipitation Measurement (GPM) mission [*Hou et al.*, 2014; www.nasa.gov/mission_pages/GPM/main]. Precipitation estimates are subject to biases and random errors that propagate into hydrologic and climatic applications ranging from flood, weather and climate analysis and prediction to budgeting water resources. The high spatiotemporal variability of precipitation poses challenges to remote-sensing systems including sensor sensitivity, its space-time resolution, the indirect nature of the measurement, and the retrieval algorithm. A variety of characteristics including intermittency, distribution of precipitation types (e.g., stratiform, convective, snow, and hail), and rates must be evaluated in order to improve the estimates and quantify their uncertainty to maximize their usability in hydrologic, climatic, and water resources applications.

Ground-based weather radar data are widely used for quantitative precipitation estimation (QPE) at fine scale (e.g., 1 km/5 min) over continental areas, but they are subject to specific uncertainties (i.e., attenuation depending on the radar frequency, ground clutter and beam blocking, variation of the reflectivity with height, conversion from reflectivity to precipitation rate, etc. See *Delrieu et al.* [2009] for a summary). The characterization of these uncertainties at fine time and space scale is highly desirable which has been motivating studies for several decades [*Zawadzki*, 1982; *Creutin et al.*, 1997; *Ciach and Krajewski*, 1999; *Ciach et al.*, 2007; *Habib et al.*, 2008; *Germann et al.*, 2009; *Villarini et al.*, 2009; *Kirstetter et al.*, 2010; *Berne and*

Krajewski, 2013]. In the context of flash floods, the causative precipitation events may develop over short space and time scales on the order of minutes and a few km, which is typically below the scales that are nominally measured by operational gauge networks [*Krajewski and Smith*, 2002; *Creutin and Borga*, 2003]. Moreover, validation of satellite QPE products from low-earth-orbiting platforms requires uncertainty estimates of instantaneous precipitation rates [*Kirstetter et al*., 2012, 2013b, 2014]. It is now recognized that uncertainty estimates of radar QPEs are necessary to realize their full potential.

Historically, radar precipitation estimates have been deterministically computed despite the known and accepted indirect and often underdetermined relation between reflectivity to precipitation rate. Since a probabilistic description of the radar QPE is most appropriate to acknowledge the possible range of estimated values, error models appeared to compensate for these limitations. Illuminating and quantifying all sources of errors separately and evaluating their joint/cumulative effects is a challenging prospect and is also dependent on the details of the radar data processing algorithms [*Jordan et al*., 2003; *Berenguer and Zawadzki*, 2008]. Recent studies empirically evaluate radar QPE accuracy with respect to an external reference for precipitation, generally based on gauge measurements, to characterize the overall uncertainty. The reference levels of uncertainty need to be significantly small compared to the radar QPE. Instrumental error and space-time representativeness limitations affect gauge estimates. The estimates must be quality-controlled and spatially interpolated for building a reference precipitation [*Ciach and Krajewski*, 1999; *Habib et al*., 2004; *Kirstetter et al*., 2010]. A number of error models have been developed with the main purpose of identifying the probability distribution and the space-time dependence of errors across various scales. The error is quantitatively decomposed into several terms [*Ciach et al*., 2007; *Kirstetter et al*., 2010; *Habib and Qin*, 2013]: (i) the unconditional bias between the radar estimates and the reference, (ii) the bias conditioned on factors like precipitation rate, accumulation period, distance from the radar, season, etc., and (iii) the random error remaining after accounting for the conditional (systematic) biases. Other features to characterize the statistical properties of the radar QPE errors are the spatio-temporal structure of the error usually described with second-order moments (correlation). These ingredients can be used to generate ensembles of probable precipitation fields by simulating random errors superimposed on the deterministic radar precipitation field [*Krajewski and Georgakakos*, 1985]. Techniques make use of LU decomposition method [*Germann et al*., 2009; *Villarini et al*., 2009] assuming the residual error follows a Gaussian distribution. Because this assumption may not be satisfied [*Mandapaka and Germann*, 2010], copulas have recently emerged as an alternative [*AghaKouchak et al*., 2010; *Villarini et al*., 2013].

However, such an approach is limited for several reasons. The concept of the error model is complex and often translates into complicated formulations. The procedure to generate the probabilistic precipitation fields follows a first diagnostic step decomposing the discrepancies into systematic and random errors, followed by a prognostic step where these (modeled) layers of information are superimposed to derive an ensemble of equiprobable precipitation fields [*Mandapaka and Germann*, 2010]. The diagnostic is often performed with variables ambiguously derived from the reflectivity factor at a coarser scale than the primary resolution of radar QPE (few minutes and kilometers) and therefore includes additional uncertainties caused by temporal/spatial resampling. Empirically evaluating the overall radar QPE uncertainty with respect to an independent reference limits the representativeness of any error characterization to the time and space domain over which it is performed. An empirical error model tends to be specific to the radar instrument (e.g., frequency, noise, and blockages), the radar algorithm, the space/time scale, and the accuracy and density of the gauge network used as a reference. As such, it has limited application for other regions, networks, countries, etc. In the context of radar QPE, the error tends to be nonstationary [*Mandapaka and Germann*, 2010]. When the empirical error model parameters are based on a long-term data sample, a relatively constant uncertainty bound is simulated for all precipitation events, despite the true variability that exists from event to event. The model should be appropriate for the event scale with the acknowledgment that there may not be a sufficiently large sample size to estimate the model parameters. No consensus exists on ways to specifically define radar errors. Some models assume a multiplicative relationship between radar QPE and gauge values, sometimes in logarithmic scale, while others are additive in that they model the error as radar QPE-to-gauge differences [see, e.g., *Tian et al*., 2013]. There are also different approaches toward modeling the distribution of error, the influence of factors primarily operative at the primary radar QPE scale like the *Z*-*R* relationship, variability of the vertical profile of reflectivity (VPR), beam blockage, etc.

With the advent of radar networks, targeting the most significant error factors becomes critical to design and characterize uncertainties in radar QPE over large areas. Classifying the data sets by multiple subsamples according to factors driving the error features can potentially lead to a generalization of the results. As an example, *Ciach et al*. [2007] investigated the influence of the seasons on the bias and the random error by dividing the radar-gauge data into hot, cold, and warm season subsamples. Characterizing uncertainties at the primary radar QPE scale would improve the representativeness of precipitation uncertainty variability at the event scale. However, reliable gauge measurements at subhourly scale are uncommon and to the best of our knowledge, no radar error model has been designed at the fine space-time resolution of the primary radar QPE scale (e.g., 1 km/5 min), close to the radar measurement itself. This temporal gap places limitations on taking advantage of the radar algorithms' capabilities to classify precipitation microphysics (e.g., precipitation typology) that present great potential for the generalization of the error characterization. As an example, the errors caused by the variability in the VPR and in the *Z-R* relationship are related due to their dependence on the underlying precipitation microphysics. This potential is increasing in the context of the upgrading of radars with dual-polarization technology, which improves hydrometeorological classification capabilities.

The aim of this study is to propose a novel approach for QPE at the primary radar QPE scale (e.g., 1 km/5 min). It is called PRORATE for probabilistic QPE using radar observations of rate and typology estimates. Probabilistic QPEs (PQPEs) are generated in acknowledgment of the possible range of values that might exist. The modeling is performed at the primary radar QPE scale to benefit from the identification of factors directly impacting the distribution of probable precipitation rate values. This approach is developed and applied on high-resolution ground radar products from the NOAA/National Severe Storm Laboratory's (NSSL) Multi-Radar Multi-Sensor system (MRMS) [*Zhang et al*., 2011a]. It yields precipitation rates over vast regions including regions of the conterminous US (CONUS) covered by Next Generation Weather Radar (NEXRAD) data (Figure 1). To our knowledge, this study constitutes the first attempt to generate Probabilistic QPE (PQPE) at such fine scale (1 km/5 min) over a continental domain. The precipitation probability maps help identify general levels of uncertainty associated with MRMS estimates. They can also be used to monitor precipitation extremes by comparing with probability exceedance of return periods. The transfer of these properties across temporal scales from 5 min to hour is examined. This study uses 1 year (August 2012 to July 2013) of MRMS precipitation products to obtain representative samples characterizing the probability distributions of precipitation rates for various conditions of rates and types. Details of the data samples, steps to refine the precipitation reference and matching procedures with radar observations are presented in section 2. Section 3 assesses the reflectivity-to-precipitation rate distribution relationships. PQPE fields, including uncertainty, probability of exceeding return periods of precipitation, aggregation, and evaluation with independent gauge observations at hourly time scale, are detailed in section 4. The paper is closed with concluding remarks in section 5.

2. Modeling Probabilistic Quantitative Precipitation Estimation

2.1. Approach and Methodology

Radar QPE algorithms generally use a reflectivity field at a constant altitude above the ground or nearest to the surface and convert it into a precipitation field by using a so-called *Z-R* relationship, occasionally conditioned by precipitation types [e.g., *Delrieu et al*., 2009; *Zhang et al*., 2011a]. In the present study, the relationship between the estimated surface reflectivity factor and the "true" precipitation rate is acknowledged to contain many factors operative at the radar measurement scale that arise from meteorological, observational, and algorithmic influences. This is conceptually described by relating the surface reflectivity factor Z to a distribution of possible precipitation rates R (Figure 2). The distribution depends on the conditioning by the aforementioned factors. The spread of the distribution—and associated uncertainty—can be attributed to factors not explicitly considered in the conditioning. Note that there is theoretically no "wrong" or "biased" estimate whatever the conditioning is, since it still reflects the actual distribution of possible rate values under these conditions. The output distribution of rates is broader when considering fewer factors. It is better defined with less uncertainty (along with the expected precipitation rates) with including additional conditioning factors. This approach assumes that the relationship between reflectivity and distribution of precipitation rate is representative and stationary (section 2.2) and that the precipitation rates can be evaluated with reasonable accuracy (section 2.3).

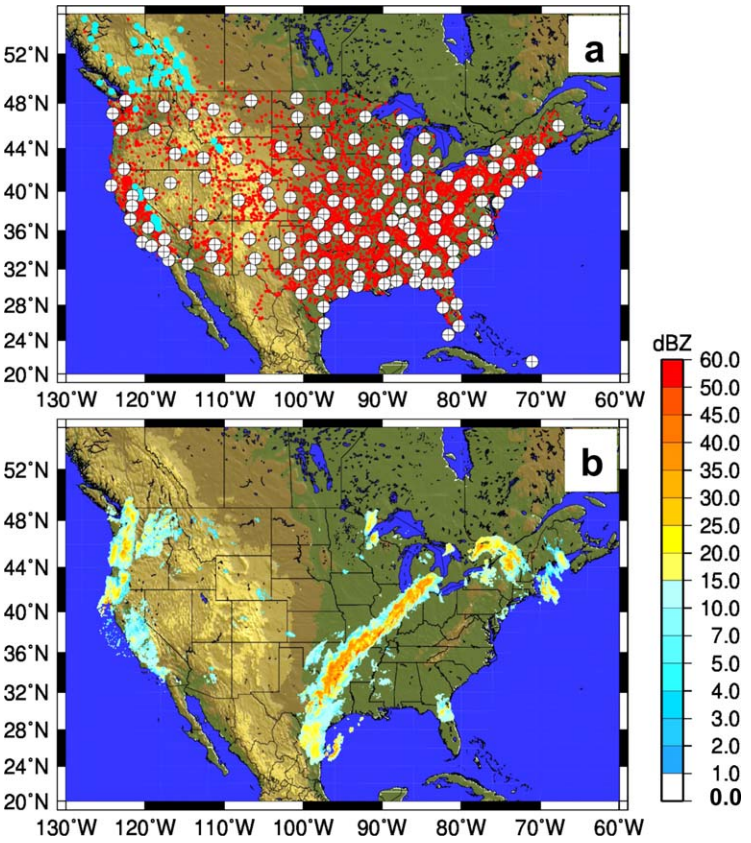

Figure 1. Map of CONUS area with (a) precipitation sensor networks used in this study: white dots represent the WSR-88D radar network, red dots represent the HADS rain gauge network, and cyan dots represent the HADS snow gauge network. (b) MRMS instantaneous reflectivity field at 0800 UTC on 11 April 2011.

The reflectivity-to-precipitation rate uncertainty approach overcomes many issues encountered in previous works. Systematic and random parts of the error are included into the distribution moments. By design this formulation yields unbiased estimates with respect to the precipitation used to build the distribution. Working at the primary radar QPE scale maintains physical (occurrence, type, and rate) and statistical (magnitude and space/time correlation) properties. The diagnostic power and prognostic capabilities of factors operative at the primary radar QPE scale are preserved (*Z-R* relationship, precipitation types, distance from the radar, radar visibility, and meteorological conditions). This enables deriving stationary characterization to be generalized over large areas or periods of time for hydrologic modeling or precipitation forecasting. Other factors than the reflectivity and precipitation types have a potential influence on the distributions as shown hereafter (section 4.4) and will be considered in the conditioning in future studies. To our knowledge, this is the first time that a radar precipitation typology (including snow and hail) is explicitly used for radar QPE uncertainty analysis.

2.2. MRMS-Based Precipitation Products

The reference precipitation $R_{ref}(A,T)$ is a proxy of the true averaged precipitation $R_{true}(A,T)$ unknown for the spatial domains A (1 km radar pixels) and time intervals T (5 min) considered for deriving the PQPE model. Since the relationship between reflectivity and distribution of precipitation should be representative, we need to characterize the variability of the reference precipitation $R_{ref}(A,T)$ for any radar observation conditions. The NOAA/NSSL Multi-Radar Multi-Sensor system [*Zhang et al*., 2011a; http://mrms.ou.edu] is a set of experimental radar products including high-resolution (1 km, 5 min) precipitation rate mosaics available over the CONUS. The calibration of the radar network is monitored by the US Radar Operating Center with the "Radar Reflectivity Comparison Data" [*Gourley et al*., 2003; http://rrct.nwc.ou.edu/rrct.html]. The MRMS system gathers information from all ground-based radars comprising the Weather Surveillance Radar—

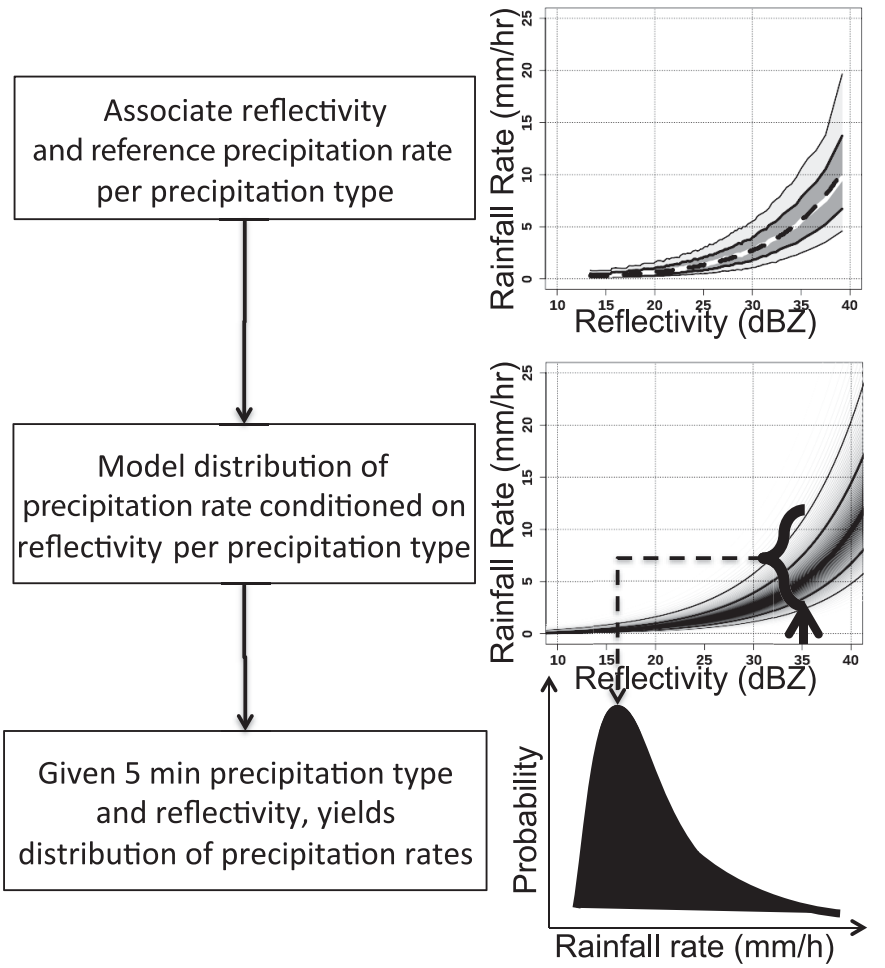

Figure 2. Flowchart of the methodology illustrated with the stratiform precipitation type.

1988 Doppler (WSR-88D) network (NEXRAD), mosaics quality-controlled reflectivity data onto a common 3-D grid and corrects for beam blockages and bright band, estimates surface precipitation accumulations and types to deliver ground-based estimates of precipitation [*Zhang et al*., 2005; *Lakshmanan et al*., 2007; *Vasiloff et al*., 2007]. The 5 min estimates rely on instantaneous radar measurements presumed to be representative of the average over the 5 min time step. The snow and rainfall gauge network is from the Hydrometeorological Automated Data System (HADS, see Figure 1a) (www.nws.noaa.gov/oh/hads/WhatIsHADS.html). The gauge network density in the eastern part of CONUS is on average one gauge per 500 km^2. Figure 1b shows an example of CONUS coverage of MRMS at 0800 UTC on 11 April 2011, highlighting several rainy systems associated with orography in the West and a mesoscale convective system associated to the 9–11 April 2011 Iowa-Wisconsin tornado outbreak.

Precipitation type-specific *Z-R* relationships are applied pixel-by-pixel on the surface reflectivity to obtain the MRMS radar-only precipitation rates. Six *Z-R* relationships are applied in MRMS, in association with the automatically detected precipitation types of stratiform rain, bright band, snow, convective rain, hail, and tropical rain [*Xu et al*., 2008] (see Table 1). The relationships for convective and stratiform echoes are used operationally in the National Weather Service. As the data sample covers a broad range of relief (Intermountain West, coasts, and plains), meteorological, weather, and observational conditions (beam blockage, altitude of the radar beam, etc.) throughout the year from a stable and uniform observation system, the sample is expected to capture many situations and ensure representativeness to document the relationship between reflectivity and distribution of precipitation rates.

Table 1. Factors of *Z-R* Relationships Applied in MRMS to the Mosaicked Hybrid Scan Reflectivity Field, and Identified From the Conditional Medians and Means of the Reference Precipitation Distributions[a]

	MRMS *Z-R* Relationships		Median *Z-R* Relationships		Mean *Z-R* Relationships	
Precipitation Types	Prefactor	Exponent	Prefactor	Exponent	Prefactor	Exponent
Stratiform	200	1.6	204	1.70	137	1.75
Convective	300	1.4	416	1.38	341	1.41
Bright band	200	1.6	97	2.31	39	2.47
Warm rain	230	1.25	305	1.3	278	1.29
Hail	300	1.4	No power model			
Snow	75	2.0	25	2.75	14.3	2.98

[a]They apply for the radar reflectivity Z in $mm^6\ m^{-3}$, the precipitation rate R (and snow water equivalent S) in $mm\ h^{-1}$. Note that the *Z-R* is capped at 55 dBZ for convective pixels, at 49 dBZ for hail pixels and at 50 dBZ for warm rain pixels.

2.3. Reference Precipitation and Matching Procedure

Reasonable accuracy for the precipitation rates is required as well as a stationary relationship between reflectivity and distribution of precipitation rate. The reference precipitation should incorporate the quantitative reliability of the gauge and the fine resolution of the radar. For this study and similarly to *Kirstetter et al*. [2012, 2014], the reference precipitation is a 5 min gauge bias-corrected MRMS product which ingests radar and gauge information. The MRMS hourly gauge-based, bias-corrected radar QPE relies on an isotropic interpolation of the residuals between hourly radar-only and hourly gauge accumulations at each gauge location. The radar-gauge residuals are spatially interpolated using an inverse-distance weighting scheme where distance weighting parameters are optimized using a cross-validation scheme [*Simanton and Osborn*, 1980]. The distance between the radar pixel and the gauges within a specified radius of the radar pixel is considered with a decreasing exponent for the distance being adjusted as a function of the number of gauges. A normal distribution to the error estimates is applied, in which the gauge impact is reduced as the distance away from that gauge increases. As a result, more weight is given to the radar estimates in areas of poor gauge coverage. A quality-control step is applied to remove gauges that strongly disagree with collocated radar observations. Finally the mapped discrepancies are superimposed to the radar-only QPE to get the hourly gauge-corrected radar QPE [*Zhang et al*., 2011a]. From *Kirstetter et al*. [2010], the critical analysis of gauge data sets is expected to increase the reliability, and the blending with radar improves the quantitative representativeness of the reference at the targeted spatial scale. The representativeness of the gauge measurement at the hourly time scale over a 1 km pixel is presumed to be high enough so the uncertainty arising from the interpolation and the effect of anisotropy in the discrepancies are minor compared to those arising from other factors affecting the radar QPE (VPR, beam blockage, etc.). The reference domains for deriving PQPE models are 1 km^2 domains matching the radar QPE pixel size and containing at least one gauge to select the highest estimation quality [*Kirstetter et al*., 2010]. The gauges used for rain are distinct from those used for snow (Figure 1a).

The radar provides the fine temporal scale required for the reference. Gauge networks sampling precipitation at 5 min resolution do not exist over areas as large as the CONUS. Furthermore, because the gauge measurement uncertainties are quite large at 5 min scale (caused by random errors in tipping-bucket measurements at low intensities, see *Ciach* [2003]), we consider the hourly time scale for reliable gauge estimates. The temporal variability is provided by the 5 min radar-only precipitation rate. Current MRMS radar products do not include a 5 min gauge-adjusted precipitation rate mosaic. Pixel-by-pixel ratios between the hourly gauge-adjusted and the hourly radar-only products are calculated, then, assuming they are stable in time, and applied as multiplicative adjustment factors to the radar-only 5 min precipitation rates. Extreme adjustment factors (outside the [0.01–100] range) caused by residual artifacts (e.g., ground clutter) are discarded and no reference is built for the PQPE. Thus, the gauge adjustment also serves as a quantitative data control procedure.

Associating different values of R_{ref} with given values of Z is performed in order to ensure as stationary relationships as possible by training the models on selected samples targeting the best-defined cases for precipitation types. Multiple precipitation regimes often coexist within a single hour and often at the same time. Consider for example a leading convective line followed by a trailing stratiform region. Since hourly precipitation accumulations are involved in deriving the reference, instances with the highest possible

Table 2. Sample Sizes for Different Precipitation Type Data Sets[a]

Precipitation Types	Sample	Training Sample
Stratiform	491,919	198,884
Convective	11,152	1,352
Bright band	53,234	16,662
Warm rain	33,576	4,850
Hail	688	674
Snow	1,118	943

[a]The training samples are used for deriving PQPE models.

proportion of a single precipitation type within 1 h (using the radar precipitation-type product at 5 min time step) are considered. All pixels under this condition in the entire study domain and all time steps in the study period are considered. The sample numbers for each precipitation type are given in Table 2.

To summarize, the reference precipitation derived at 1 km/5 min scale from gauge and radar data is matched with the automatically detected precipitation type and the estimated surface reflectivity factor to constitute samples used for deriving PQPE models.

3. Conditioned Distributions of Precipitation Rates

3.1. Empirical Distributions

Figure 3 shows the reference precipitation rate distributions as functions of the equivalent reflectivity factor for the different MRMS precipitation-type classes. The 50%, 25–75%, and 10–90% quantiles have been computed for the precipitation rate distributions and are plotted in the figure. Figures 3a–3f show a shift toward higher precipitation rates as the reflectivity increases in line with expectations. This rate of increase is more pronounced with MRMS-classified convective, tropical, and hail echoes (Figures 3d–3f) and lower for the

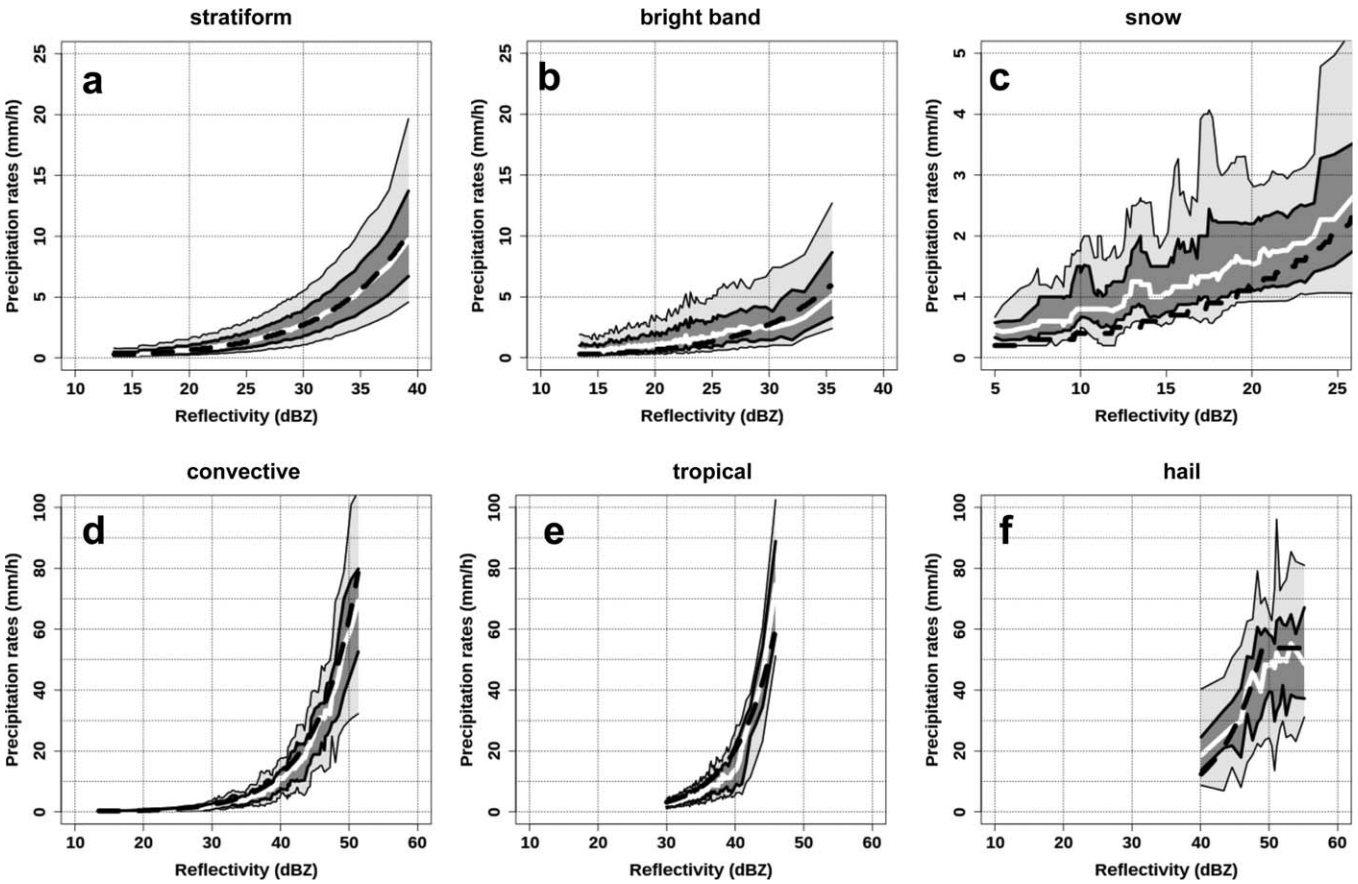

Figure 3. Reference precipitation rate distributions as functions of the equivalent radar reflectivity for (a) stratiform, (b) bright band, (c) snow, (d) convective, (e) tropical, and (f) hail types. The thick white line represents the median (50% quantile), the dark gray-shaded region represents the area between the 25% and 75% quantiles, and the light gray-shaded region represents the area between the 10% and 90% quantiles. The black dotted line represents the typed *Z-R* relationship used in the MRMS algorithm. Note that the horizontal and vertical axis scales differ among the subfigures.

stratiform, bright band, and snow echoes (Figures 3a–3c). The spread of each distribution increases with the reflectivity values as well. This feature, addressed in more detail below, indicates larger uncertainties (heteroscedasticity) in quantifying the precipitation rates with increasing reflectivity factors.

Figures 3a–3f also plots the MRMS *Z-R* relation that is used for each precipitation type (see Table 1 for the prefactors and exponents of these relationships). For the most part, the *Z-R* curves lie within the [25–%75%] interquantile of the empirical reference rates. They are very close to the median for the convective (NEXRAD relationship, Figure 3d) and stratiform (Marshall-Palmer relationship, Figure 3a) classifications. This proximity for two significant precipitation types (these two classifications represent 76% of the global data sample) is an indication of the satisfactory computing of the reference and conditional distributions. It does not however guarantee that the reference perfectly matches the true precipitation. Eliminating systematic biases is a necessary and important condition to improve confidence in our reference precipitation.

The Marshall-Palmer relationship is used for both stratiform and bright band types. For echoes taken within the bright band, the difference between the MRMS *Z-R* relationship and the empirical median is more significant with underestimation of precipitation for *Z* values below 20 dBZ (∼75% of the reference distribution being above the relationship) and overestimation of precipitation at *Z* values above 33 dBZ (∼60% of the distribution being below the relationship). These differences illustrate the benefit of identifying specific precipitation microphysics in order to adapt the quantitative estimation scheme to different DSD types. Similar departures are noted for hail, which is not a surprise as this precipitation type is difficult to characterize and quantify. A significant overestimation can be noted for the tropical case (note that reflectivity values below 43 dBZ includes 95% of the sample). This is consistent with the identified impact of the tropical type on overestimation of precipitation accumulations by MRMS [*Chen et al*., 2013]. One of the most significant departures between the MRMS *Z-R* relationship and reference distributions is for snow. The snow water equivalent (SWE) relationship is predominantly below the 25th percentile of the reference distribution, indicating a very significant underestimation of snow rates. Research is active in this area, and physical parameters such as density and temperature need to be accounted for in order to improve SWE estimation by active remote sensing.

Figure 4 sheds more light on the behavior of the biases between the MRMS *Z-R* relationships and the distributions of reference precipitation, as well as on the uncertainties in quantifying precipitation rates. Each point represents the values of bias or relative uncertainty computed from data associated to a bin of reflectivity. In Figure 4a, the relative bias is computed at percentiles of reflectivity values as the relative difference in percent between the deterministic MRMS *Z-R* relationship rate, denoted "*ZR*," and the conditional mean of the reference distribution, denoted *m*

$$Bias\ (Z) = 100\frac{ZR - m}{m}. \tag{1}$$

The relative uncertainty (Figure 4b) is computed as the interquantile range [25%–75%] of the distribution normalized by the mean

$$Uncertainty\ (Z) = 100\frac{q75 - q25}{m}, \tag{2}$$

with q_{25} and q_{75} being the 25th and 75th percentiles of the reference distribution conditioned on *Z*, respectively.

Deterministic MRMS tends to underestimate lower precipitation rates associated to echoes below 30 dBZ (Figure 4a). Biases are as low as −60% below 20 dBZ with bright band and snow types and are more moderate for the stratiform precipitation type (−25%). The Marshall-Palmer relationship yields significant underestimation of rates associated to bright band echoes (from −10% to −60%). This might relate to a VPR impact in addition to the MRMS Z-R relationship. The same relationship performs much better with stratiform echoes. The SWE relationship shows underestimation from −60% at 10 dBZ to −10% at 23 dBZ. Note that up to 30 dBZ, all conditional biases are increasing functions of the reflectivity factor. In the range 30–50 dBZ, the convective and stratiform biases are within 20%. The overestimation is confirmed for tropical echoes with most of the bias values between 15% and 50%. It is more moderate for hail. Note that above 30 dBZ there is no clear trend for the biases with reflectivity factor. However, the biases differ considerably depending on the precipitation types.

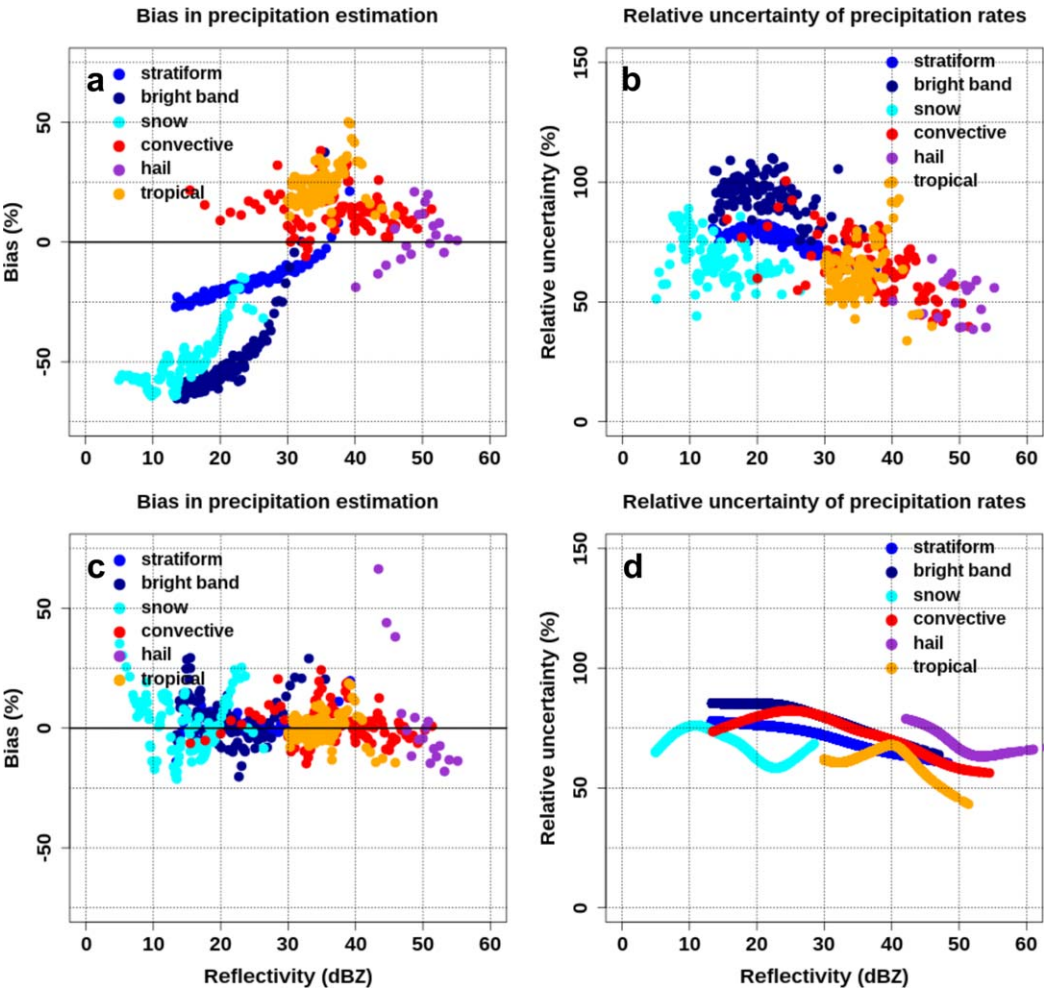

Figure 4. (a) Relative biases between the MRMS precipitation estimates and the reference precipitation as functions of the equivalent radar reflectivity. (b) Relative uncertainty in the reference precipitation estimates as functions of the equivalent radar reflectivity. (c) As in Figure 4a but for the PQPE models. (d) Relative uncertainty in the fitted PQPE models as functions of the equivalent radar reflectivity.

The uncertainty in quantifying precipitation rates strongly depends on the type and the magnitude of the reflectivity (Figure 4b). The absolute uncertainty, denoted by the spread of the distributions in Figure 3, is a systematically increasing function with the reflectivity factor. Yet the absolute uncertainty does not increase as fast as the averaged rates, so the relative uncertainty is generally a decreasing function of the reflectivity factor following normalization in (2). The fact that relative uncertainties are generally larger than the biases supports the use of probabilistic QPE values to acknowledge this feature. The largest uncertainties are found with the bright band echoes with values as high as 110% around 20 dBZ. It drops for higher reflectivity values toward 75% uncertainty at 35 dBZ. The convective echoes present large uncertainties as well, ranging from more than 90% at 25 dBZ to less than 50% at 50 dBZ. For $Z > 45$ dBZ, hail is the precipitation type estimated with the lowest precipitation rate relative uncertainties (around 50%). Tropical precipitation estimation shows relative uncertainty in the range 50–75%, as well as snow. Convective and stratiform echoes show significant reduction of the uncertainty with increasing reflectivity, e.g., from $\sim$80% at 15 dBZ to $\sim$55% at 35 dBZ for stratiform.

It is noteworthy that the Marshall-Palmer relationship presents both reduced biases and uncertainties when applied on stratiform type compared to the bright band echoes. It may be a more accurate model of conversion from the radar signal to precipitation rate for the stratiform precipitation microphysics. The bright band type represents areas where any part of the radar hybrid scan beam intersects the melting layer, defined by a combination of radar-derived bright band top/bottom heights and freezing level height. It includes radar samples partially or completely in the snow/ice region above the melting layer while the

surface precipitation is rain. Similar negative biases in the bright band and snow echoes (Figure 4a) most likely reflect these cases. Further, this group also includes radar samples within the bright band or partially below the bright band, thus the largest relative uncertainties (Figure 4b) in the radar QPE. Convective precipitation is characterized by a larger microphysical variability than with stratiform precipitation. The large variability especially with high precipitation rates indicates uncertainty with the assumed DSDs and raises questions about the use of a unique *Z-R* relationship. Overestimation associated with tropical echoes has been related to erroneous tropical precipitation delineations in areas of mesoscale convective systems in MRMS. The moderate biases and uncertainties obtained with the tropical and hail types also illustrate the benefits in segregating different precipitation types and applying specific *Z-R* relations. The significant biases observed with snow reveals the lack of research performed with this particular precipitation type in relation to the others and is an active area of current research.

3.2. Modeling

Probabilistic QPEs computed in this study are modeled from the conditional distribution of precipitation rate for given precipitation type and radar reflectivity factor. For each type, the conditional distribution $R_{ref}|Z$ is parameterized to a simple theoretical model. For the sake of formulation efficiency, a number of conditional densities with the first two moments as parameters are considered here: the mean describing the average *Z-R* relationship and the standard deviation. This eases the application in deriving various products and generating ensembles of precipitation rates. We assume the distribution has the same parametric form for all radar reflectivity factor values within a given type by using the generalized additive models for location, scale, and shape approach (GAMLSS) [*Rigby and Stasinopoulos*, 2005]. To evaluate the most appropriate model, the goodness of fit has been checked by investigating different parametric density fits (e.g., normal, lognormal, gamma, Weibull, logistic, etc.) for reference subsamples corresponding to the neighborhood of a selected reflectivity bin, as described in *Ciach et al*. [2007]. Such checks have been performed for different reflectivity values and all precipitation types. The distributions of R_{ref} (not shown here) were generally found to be unimodal and asymmetric, making the Gaussian model inappropriate. While the Reverse Gumbel and the inverse Gaussian models are found to provide best fits on some instances, the lognormal was consistently found to be the best overall for stratiform, bright band, and snow types. The gamma model was found more appropriate for convective, tropical, and hail. The lognormal and gamma distributions present the advantage to be defined with positive values only, which avoids potential negative precipitation rates when generating ensembles of precipitation [*Ciach et al*., 2007; *Villarini et al*., 2013]. More complex models could be evaluated, such as mixtures of distributions to improve the flexibility of the distribution model. These would be justified if additional factors driving the distribution features were considered, such as the radar sampling conditions, distance from the radar, temperature for snow, etc. These aspects will be analyzed in future studies. In this prototype study, we strike a balance between model complexity, accuracy, and efficiency.

Additional tests on the R_{ref} distributions were performed on the whole data set for each precipitation type by using the GAMLSS technique. As a preliminary step, Z is considered as the main driving (explanatory) variable conditioning the PQPE. Generalized linear models for location, scale, and shape aim at modeling the parameters of a response variable's distribution (R_{ref}) with the following assumptions: (1) R_{ref} is a random variable following a known distribution with density $f(R_{ref}|\mu,\sigma)$ conditional on the parameters (μ,σ) and (2) the observations R_{ref} are mutually independent given the parameter vectors (μ,σ). Each parameter is a function of Z using monotonic (linear/nonlinear or smooth) link functions. GAMLSS is best fit using the package GAMLSS [*Stasinopoulos and Rigby*, 2007] in R [*R Development Core Team*, 2012]. Except for the case of hail, the precipitation trends for each parameter are fitted using a power law relationship, consistent with the classical *Z-R* formulation. In the case of hail, Figure 3d shows that, unlike other precipitation types, the conditional distribution of precipitation rates is not continuously increasing with reflectivity factor. This is attributed to the uncertainty in quantifying hail precipitation rates with single polarized radars. Cubic splines with 3 degrees of freedom were used to model hail precipitation trends for each parameter of the distribution. A variety of two-parameter distributional forms (not shown) were also tested. The goodness of fit on the whole data set has been checked for each of the density fits by investigating the Akaike information criteria (AIC), computing the residuals, first four moments, their Filliben correlation coefficient, and quantile-quantile plots [*Stasinopoulos and Rigby*, 2007]. The results confirmed the findings above that is the

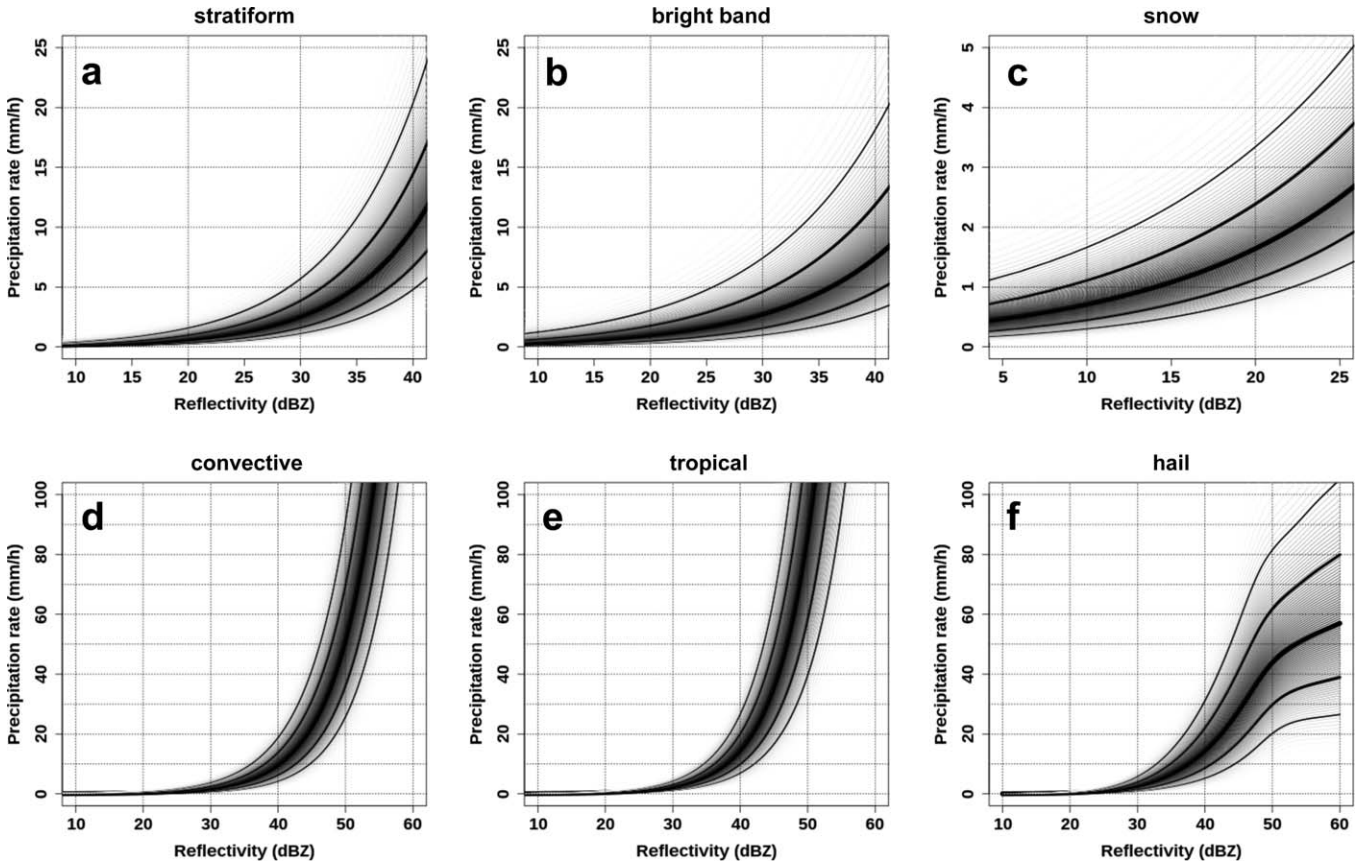

Figure 5. Models for precipitation rate distributions conditioned on the equivalent radar reflectivity for (a) stratiform, (b) bright band, (c) snow, (d) convective, (e) tropical, and (f) hail types. The thick black line represents the median (50% quantile), the dark gray-shaded region represents the area between the 25% and 75% quantiles, and the light gray-shaded region represents the area between the 10% and 90% quantiles.

lognormal model for stratiform, bright band, and snow, and the gamma model for convective, tropical, and hail were most appropriate for describing the variability exhibited by the data

$$f(R_{ref}|\mu,\sigma)=\frac{1}{R_{ref}\sqrt{2\pi}\sigma}e^{-\frac{(\ln R_{ref}-\mu)^2}{2\sigma^2}} \quad \text{for the lognormal model,} \tag{3}$$

$$f(R_{ref}|\mu,\sigma)=\frac{1}{(\sigma^2\mu)^{\frac{1}{\sigma^2}}}\frac{R_{ref}{}^{\frac{1}{\sigma^2}-1}e^{\frac{-R_{ref}}{\sigma^2\mu}}}{\Gamma\left(\frac{1}{\sigma^2}\right)} \quad \text{for the gamma model.} \tag{4}$$

Using the distributions, the location parameter μ is related to the deterministic component of the *Z-R* relationship and the scale σ is related to the variability of this relationship. Both depend on the magnitude of the reflectivity factor *Z*, in order to account for the shift toward higher precipitation rates and for increasing uncertainty (heteroscedasticity) with the reflectivity factor (Figure 3). These models are compact and simple as described with rather simple mathematical expressions, which minimizes computational costs.

The modeled conditional distributions of precipitation rates are plotted for each type in Figure 5. They present visual consistency, and particularly account for the proportionality of precipitation uncertainty to the magnitude of the reflectivity factor. Their consistency is checked in terms of relative bias and uncertainty compared to the empirical distributions in Figure 3. A representative *Z-R* relationship needs to be extracted from the conditional distributions. In case of a nonsymmetric distribution, the median can be considered, as it seems close to the stratiform and convective *Z-R* relationships used in MRMS (Figures 3 and 5). Yet, as the first moment of the distribution, the expected value $E(R_{ref}|Z)$ is used to compute the relative bias.

Z-R relationships are computed from the conditional medians for each precipitation type except for hail (Table 1). The coefficients of the stratiform relationship are similar to the deterministic MRMS relationship.

Table 3. Relative Bias Between the Precipitation Rate Estimates Using MRMS *Z-R* Relationships, and Identified From the Conditional Medians and Means of the Reference Precipitation Distributions

Precipitation Types	MRMS *Z-R* Relationships	Median *Z-R* Relationships	Mean *Z-R* Relationships
Stratiform	−10.2%	−16.5%	2.18%
Convective	11.5%	−9.86%	−0.4%
Bright band	−42.0%	−27.3%	2.55%
Warm rain	24.1%	−9.68%	−1.17%
Hail	2.05	−8.32	0.82
Snow	−46.2%	−15.9%	0.28%

This is further confirmation that no significant bias affects the conditional distributions and their modeling. As anticipated, the bright band and snow relationships differ from their MRMS deterministic counterparts with prefactors as twice as low and higher exponents. Their similarity most likely reflects the fact that the bright band type includes radar samples partially or completely in the snow/ice region above the melting layer. The warm rain prefactor is higher and closer to the convective relationship. Again the need to differentiate distinct microphysical regimes within the precipitation field observed by the radar is highlighted by the specific relationships associated to each precipitation type. In particular the "median" bright band relationship exhibits very different coefficients from the Marshall-Palmer relationship used in MRMS.

Mean *Z-R* relationships are computed from the conditional means for each precipitation type except for hail (see Table 1). Relative biases are computed using these newly derived relationships. As shown in Figure 4c biases are significantly reduced for each precipitation type compared to the biases associated to the deterministic MRMS relationships in Figure 4a. Table 3 compares the overall biases values obtained with the default MRMS relationships and with the mean *Z-R* relationship for each precipitation type. While the MRMS stratiform and convective biases are within 12%, significant departures are noted with specific relationships for bright band, warm rain, and snow precipitation types. All biases are reduced within 3% when applying the mean *Z-R* relationship. As can be expected the mean *Z-R* relationship is more appropriate than the "median" *Z-R* relationship for quantitative precipitation estimation. In fact, the median takes on lower values than the expected value for unimodal positively skewed distributions. As such, the Marshall-Palmer relationship, which is close to the corresponding stratiform "median" *Z-R* relationship (Table 1), causes precipitation underestimation. Figure 4d shows the relative uncertainty obtained with the modeled conditional distributions. The models represent quite satisfactorily the uncertainty, yet some underestimation for the stratiform and bright band echoes and overestimation for hail can be noted. It can be attributed to the choice of a simple two-parameter distribution model.

4. Validation and Applications

The following section applies the PRORATE framework to mesoscale convective systems, which are common over the Great Plains of the US during the warm season. Figure 1b shows a frontal system that extends from North Texas to Michigan during the 9–11 April 2011 Iowa-Wisconsin tornado outbreak, which produced 42 tornados over five states. Figure 6 shows the radar hybrid scan reflectivity (Figure 6a) and associated precipitation-type field (Figure 6b) at 0800 UTC on 11 April 2011. Convective cores are embedded in a broad stratiform region, and the MRMS algorithm classified some of the most active cores as tropical. Figure 6c shows the map of conditional mean derived from the PQPE model, and Figure 6d shows additive difference between the PQPE mean and the radar-only instantaneous precipitation rate from MRMS. This derived QPE field is computed in a very similar way to MRMS by considering the reflectivity and the precipitation type at every pixel. The precipitation rate density function is derived by applying the relationships $PQPE = f(Z, type)$ (Figure 5).

4.1. Relative Uncertainty Maps

One potentially useful application of the PQPE method is the generation of relative uncertainty products at the MRMS precipitation rate scale (1 km/5 min). For a given radar pixel characterized by a reflectivity factor and precipitation type, any quantile can be extracted from the corresponding conditional distribution of the precipitation rates. The cumulative distribution function *CDF* is defined in the interval [0,1] and represents the probability p that the precipitation rate R_{ref} takes on a value less than or equal to a given threshold rate $R_{threshold}$. It is defined as follows:

$$CDF(R_{threshold}) = \frac{1}{2} + \frac{1}{2} erf\left[\frac{\ln R_{threshold} - \mu}{\sqrt{2}\sigma}\right] \quad \text{for the lognormal distribution,}$$

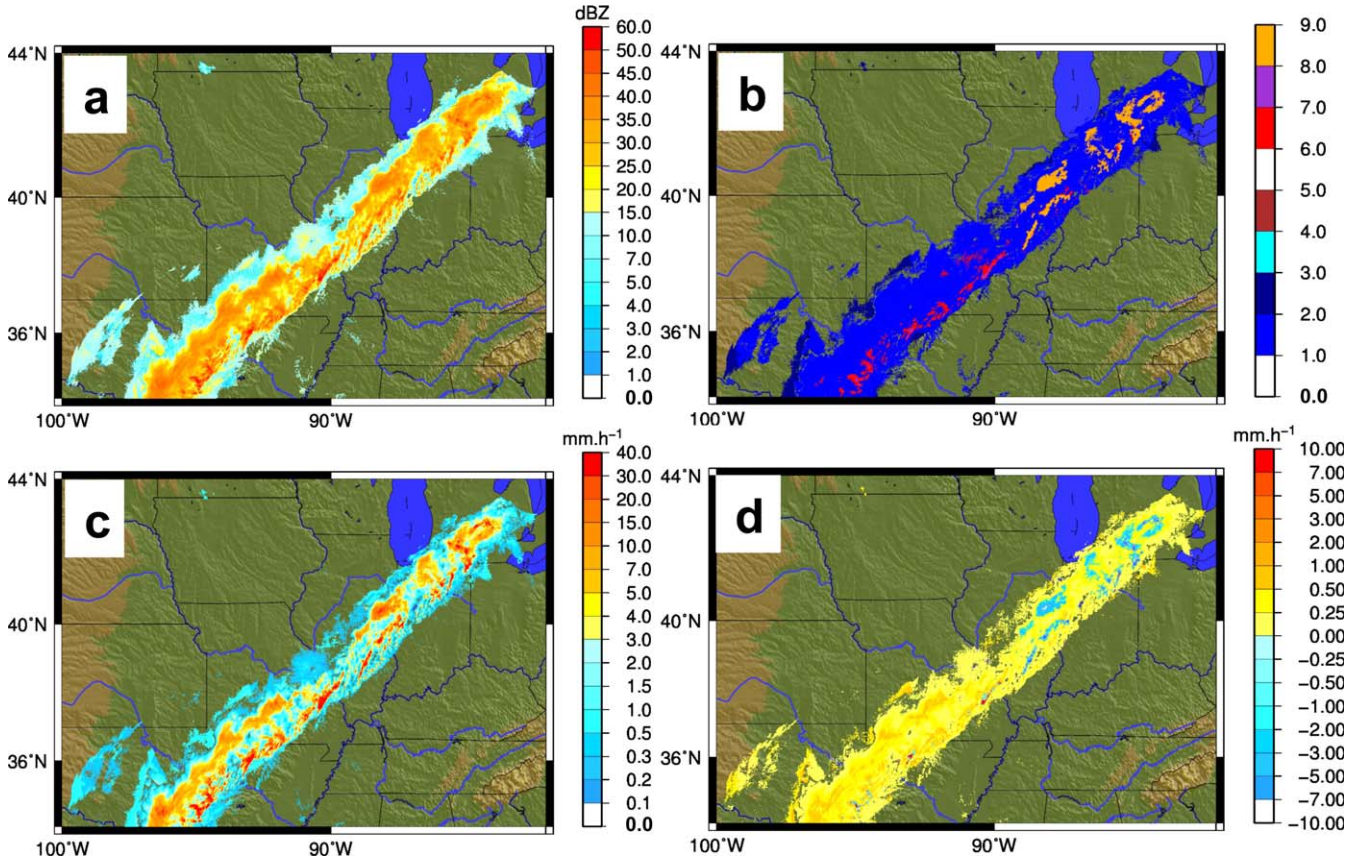

Figure 6. Example of frontal system at 0800 UTC on 11 April 2011 near Michigan: (a) radar hybrid scan reflectivity, (b) precipitation-type fields (1: stratiform, 2: bright band, 3: snow, 6: convective, 7: hail, and 9: tropical), (c) PQPE mean from the model, and (d) difference PQPE mean-MRMS radar-only 5 min QPE.

$$CDF(R_{threshold}) = \frac{1}{\Gamma\left(\frac{1}{\sigma^2}\right)}\gamma\left(\frac{1}{\sigma^2}, \frac{R_{threshold}}{\sigma^2\mu}\right) \quad \text{for the gamma distribution,}$$

with *erf* the erf function, Γ is the gamma function, and γ the lower incomplete gamma function. The conditional quantile function q is the inverse cumulative distribution function $q = CDF^{-1}(p)$ and relates a threshold rate to a given probability that the precipitation rate R_{ref} takes on a value less than or equal to this threshold (see Figures 3 and 5). The conditional median is the fiftieth percentile and is noted q_{50}.

The relative uncertainty is defined in equation (2) as the interquantile range 25%–75% normalized by the mean. Figure 7 shows the impact of precipitation classification and adaptive PQPE relationships on the radar QPE relative uncertainty. As noticed in Figure 4 the relative uncertainty is generally above 50% and within 80%, and is marked by a significant conditioning on the precipitation type. In comparing Figures 7 and 6, we see the areas with lower relative uncertainty correspond to convective and tropical precipitation types and cores with higher precipitation rates. These features illustrate the impact of specific precipitation microphysics on the quantitative estimation.

4.2. Return Period Exceedance

Another useful application of the PQPE model is the computation of the probability of exceeding established precipitation return periods. This is useful for monitoring precipitation extremes that may lead to flooding. The probability of exceedance of some predetermined threshold $R_{threshold}$ is computed as $P(R_{ref} > R_{threshold}) = 1 - CDF(R_{threshold})$.

As an example application, we incorporate precipitation return period maps for 2 and 10 years (Figures 8a and 8b, respectively). Both correspond to 5 min precipitation rates. The return period maps are derived from atlases of precipitation frequency estimates from the NOAA's National weather Service Hydrometeorological

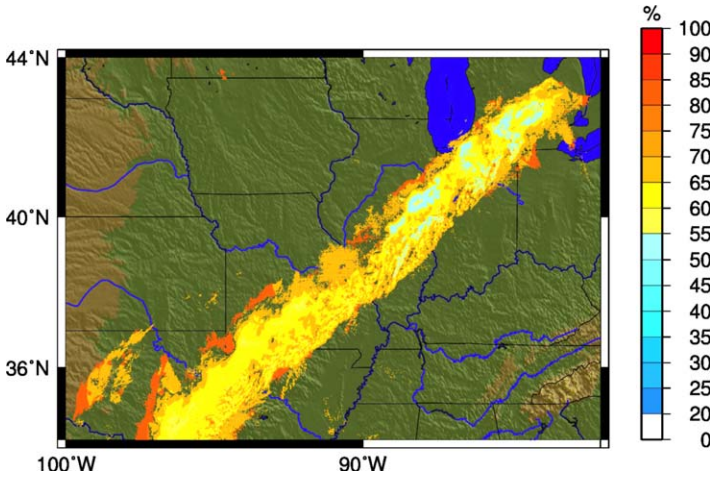

Figure 7. Relative uncertainty maps for the PQPE field at 0800 UTC on 11 April 2011 at 5 min time scale.

Design Studies Center (http://hdsc.nws.noaa.gov/hdsc/pfds/index.html). Precipitation frequencies are available for longer accumulation periods (e.g., hourly) and higher precipitation rate thresholds (e.g., 100 year). Figures 8a and 8b show higher precipitation amounts in the southeastern part of the U.S. and are related to tropical cyclones from the Atlantic Ocean and Gulf of Mexico, frontal thunderstorms and air mass thunderstorms during the warm season. Figures 8c and 8d show the corresponding maps of probabilities of exceedance by comparing the conditional distributions to the precipitation return period. In comparing Figure 6 and Figures 8c and 8d, we see higher probability of exceedance corresponds to the high precipitation rate cores, as we would expect. These products are of interest for monitoring flash floods because they quantify the probability of exceeding specific precipitation rates at commensurate space and time scales at which these events occur. They are of particular interest for the Flooded Locations And Simulated Hydrographs Project (FLASH) (http://flash.ou.edu), which ingests MRMS precipitation rates. Future work will examine these precipitation products in the context of observed flash flooding.

4.3. Temporal Accumulation

Owing to its rather simple formulation, the PQPE fields can be efficiently computed at the MRMS time scale of 5 min. Temporal accumulation of PQPE is needed for evaluating the propagation of the uncertainty at coarser time scales and computing the probability of exceeding precipitation amounts associated to return periods at these scales.

The temporal correlation is an essential property of precipitation. It impacts on the accumulation of PQPE, especially the spread of the accumulated distribution. Note that the expected value is not affected. While an extensive analysis of this impact goes beyond the current scope of the study, we assume two extreme cases to illustrate it: two successive PQPE fields are assumed either independent or totally correlated. In the first case, the probability distribution of the sum of two independent random variables is the convolution of their individual distributions. The hourly accumulations are obtained by convoluting 12 successive 5 min probability density fields of precipitation rate. This computation is performed with the package "distr" [*Ruckdeschel et al*., 2006] available in R. For the correlated case, hourly accumulation is performed by quantiles of the distributions. Accounting for this (positive) correlation between distributions results in a broader aggregated distribution. Figure 9 shows the hourly PQPE mean (Figure 9a), along with the additive differences with the MRMS hourly radar-only (Figure 9b) and gauge-corrected (Figure 9c) QPEs. The PQPE mean field is obtained by accumulating the 5 min PQPE fields from 0705 UTC to 0800 UTC on 11 April 2011. Identical results are obtained whatever the temporal correlation (not shown here). The lower rates at the borders of the precipitation fields present slightly higher values than the radar-only estimates, corresponding to the correction of underestimation noticed for lower reflectivity echoes (section 3.1 and Figure 4). The highest rates are reduced compared to the radar-only QPE, presumably correcting the overestimation caused by the tropical Z-R relationship (Figures 4a and 6b). The difference with the gauge-corrected radar field shows the impact of the blending technique between radar and gauge precipitation, which is isotropic and does not account for the significant anisotropy of the precipitation field [*Kirstetter et al*., 2010; *Delrieu et al*., 2014.]

The PQPE presents the advantage of providing the uncertainty associated to its estimates. Similar to section 4.1, the relative uncertainty for the hourly precipitation is derived from the PQPE and shown in Figure 10.

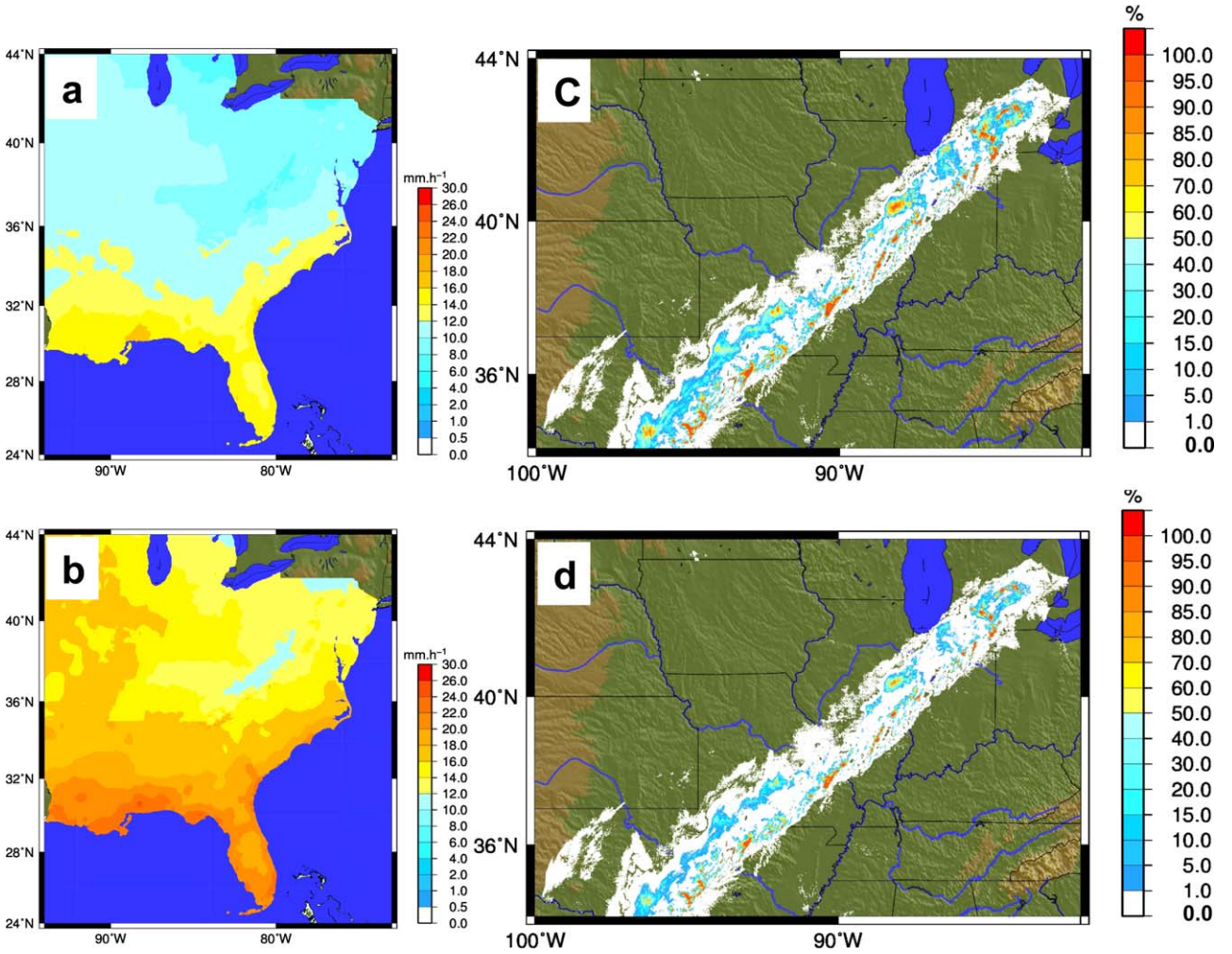

Figure 8. Maps of (a) 2 years and (b) 10 years precipitation rates return periods at the 5 min time scale; probability of exceedance of the (c) 2 years and (d) 10 years return periods for the PQPE field at 0800 UTC on 11 April 2011.

With assuming no temporal correlation (Figure 10a) the uncertainty values range between 20% and 50% and are significantly lower than the equivalent at 5 min scale. The uncertainty values are larger and similar to the 5 min scale when assuming temporally correlated 5 min PQPE fields. Figures 10c and 10d show the corresponding maps of probabilities of exceedance by comparing the hourly distributions to the hourly precipitation return period. Higher probability of exceedance corresponds to higher uncertainties (spread of the distributions), as we would expect.

4.4. Validation

While some insights are provided at the 5 min time scale in section 3.1 and Figure 4, an indirect validation of the PQPE model evaluates its transferability to a greater temporal scale, one that has reference precipitation with much greater accuracy. It is restricted to the hourly gauge-corrected radar QPE over 1 km^2 pixels that contain at least one gauge within them to select the highest reference quality. The gauges used for rain validation are distinct from those used for snow validation (Figure 1). Multiple precipitation regimes often coexist within a single hour. An independent data set is therefore provided by the instances with several precipitation types within 1 h (using the radar precipitation-type product at 5 min time step). The 5 min PQPE estimates are accumulated at the hourly time scale and compared to this hourly reference. The sample size is 57,707 for rain and 1118 for snow. We provide here a validation of two major features of the PQPE model: the systematic biases and the spread.

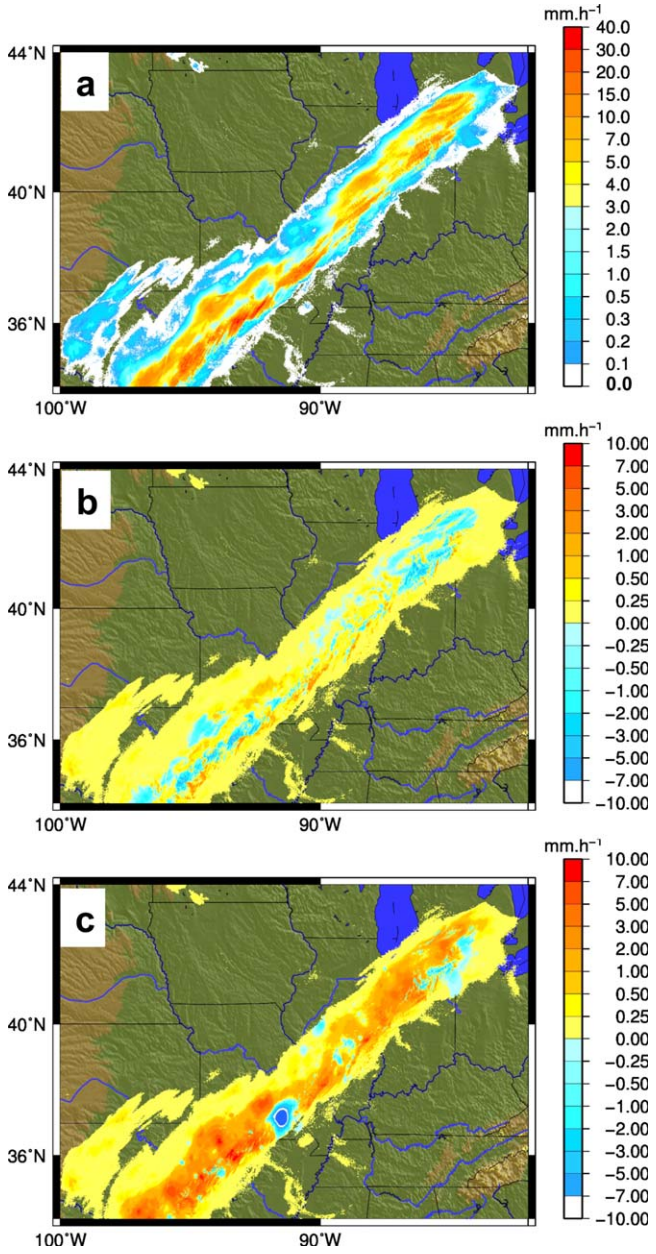

Figure 9. PQPE (a) hourly mean, (b) difference mean PQPE-MRMS hourly radar-only QPE, and (c) difference mean PQPE-MRMS gauge-corrected QPE at 0800 UTC on 11 April 2011.

For the biases the PQPE is compared to the radar-only QPE. The biases in estimating precipitation rates at 5 min interval (Figures 4a–4c) propagate up to the hourly time scale. As a result for precipitation, while the radar-only and the hourly PQPE present similar correlation coefficients with the reference (0.80), the PQPE presents a very small relative bias (−0.72%) compared to an already good score obtained with the radar-only product (−1.8%). Because compensation effects could eliminate systematic biases linked to the occurrence of various precipitation types within the hour, the biases are also evaluated with conditioning by the proportion of precipitation-type occurrence within the hour (Figure 11). The bright band precipitation type is shown to negatively impact the hourly MRMS radar-only product. The underestimation noted in section 3.1 propagates up to the hourly time scale. The tropical precipitation type causes overestimation in the MRMS radar-only product, also noted in *Chen et al.* [2013]. In all cases, the PQPE amounts present lower departures from the reference compared to the default MRMS radar-only products. The improvement is particularly significant for the tropical and bright band types. It can therefore be claimed the distributions of precipitation rate are representative at the first order. While an indirect validation, these results confirm that the proposed formulation provides less biased estimates by adapting to the radar precipitation typology at the estimation scale with benefits that propagate up to the hourly scale.

The uncertainties associated to the hourly PQPE estimates are quantified and their distribution is shown with assuming either independence between 5 min PQPE (Figure 12a) or correlation (Figure 12b). As expected with assuming no temporal correlation the uncertainty values (20%–50% range) are lower than with assuming temporally correlated 5 min PQPE fields (50%–85% range). To test how well the distribution of the hourly QPE represents the true variability (uncertainty) of the reference, the rank histogram of the hourly reference is computed with respect to the ensemble QPE. This graphical method illustrates where the reference falls in the distribution function *CDF* of the PQPE estimate. In a distribution with perfect

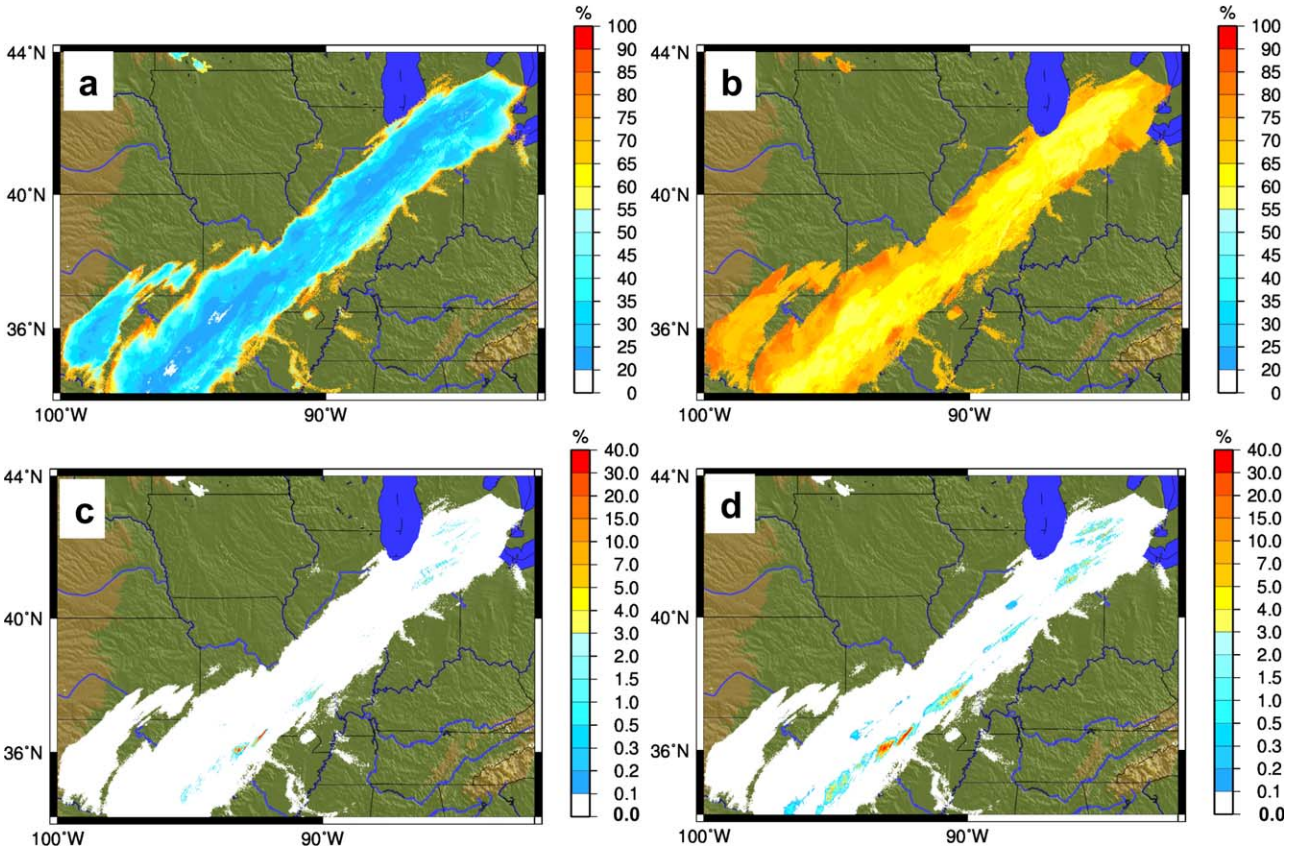

Figure 10. Maps of relative uncertainty at hourly time scale with assuming (a) no correlation and (b) total correlation between 5 min PDFs; probability of exceedance of the 2 years return periods with assuming (c) no correlation and (d) total correlation between 5 min PDFs for the PQPE field at 0800 UTC on 11 April 2011.

spread, each quantile represents an equally likely scenario for the reference. The perfect case is a flat rank histogram indicating that the reference probability distribution is well represented by the PQPE distribution. The U-shaped histogram shown in Figure 12c indicates that the spread of the hourly PQPE distribution assuming temporal independence is too small, or underdispersive. A significant number of observations fall outside the extremes of the PQPE distribution. The histogram obtained with assuming temporal correlation present much better shape in Figure 12d, even if some low observed values fall outside of the low extremes of the PQPE distribution. This result shows that assuming temporal correlation between 5 min PQPE is more realistic than assuming that successive fields are independent. Additional analysis is needed regarding the correlation, which probably depends on precipitation type, location in storm system, velocity of the weather system, etc. Therefore, higher levels of representativeness remain to be evaluated. This aspect will be addressed in future studies. Also, many factors operative at the radar measurement scale like DSD, VPR, beam blockage, storm life cycle, dryness of the subcloud layer, etc. are not currently considered and may have a diagnostic power for this result (section 2.1).

5. Discussion and Conclusion

Since errors impacting QPE by weather radar are complex and often difficult to disentangle, a probabilistic approach for estimating precipitation from a radar measurement can effectively reduce systematic biases and communicate the uncertainty bounds to users. In this study, we propose the new method PRORATE to derive probability distributions of precipitation rates instead of single values using a model quantifying the relation between radar reflectivity and the corresponding reference precipitation. The PQPE method explicitly accounts for precipitation types (including solid precipitation) that are automatically detected in the MRMS system. The most distinguishing characteristic of the method is its capability of yielding PQPEs and derived fields at the native resolution of 1 km/5 min. By design the PQPEs are conditioned on the

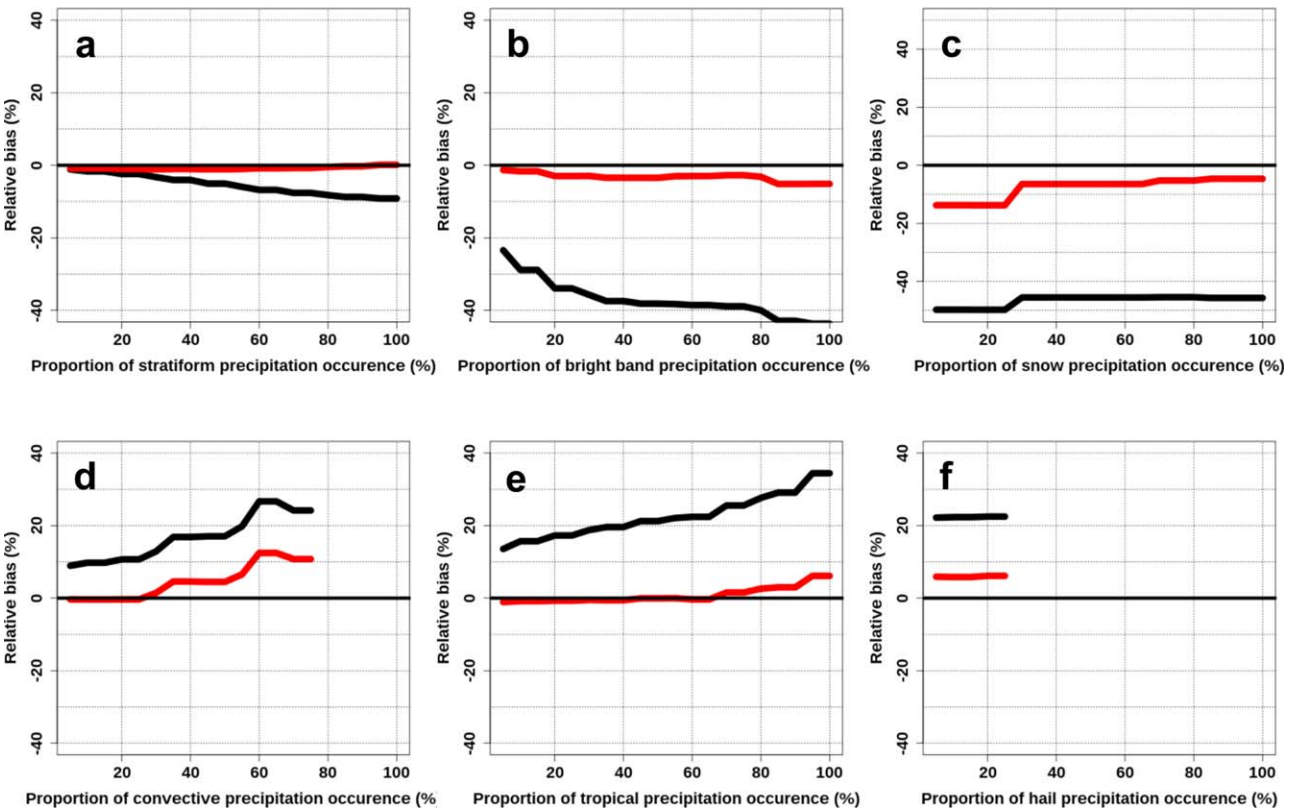

Figure 11. Relative bias in percent for the MRMS radar-only hourly QPE (black) and the hourly PQPE mean (red) for (a) stratiform, (b) bright band, (c) snow, (d) convective, (e) tropical, and (f) hail types as functions of the proportion of rain-type occurrence within the hour.

distribution of driving factors directly related to the instrument measurement and drop size distribution variability. A quantitative diagnostic was performed on the MRMS *Z-R* relationships in terms of biases and uncertainty. Systematic biases were found to be significant for echoes that were measured in the bright band, for snow, and for those that were deemed to be from tropical precipitation. The conditional distributions of precipitation rates are shown to significantly reduce these systematic biases while quantifying the remaining uncertainty. Examples are presented to show how the PQPE method can be combined with pre-established precipitation rate thresholds to monitor the probability of precipitation extremes that may lead to flash flooding. The transferability of the models at the primary radar QPE scale was tested by aggregation to hourly scale. Good performances were noticed in terms of reducing systematic biases. It was also shown that assuming temporal correlation between 5 min PQPE is more realistic than assuming that successive fields are independent.

For future work, we will revisit key assumptions. First, the distribution is currently supposed to have the same parametric form for all radar reflectivity factor values within a given type. While current distributions are reasonably representative at the first order, higher levels of representativeness still remain to be evaluated. More sophisticated models for the distribution of precipitation rates will be investigated. Second, as a more refined conditioning allows better distinguishing distributions, additional factors beyond reflectivity value and precipitation type can be employed in the PQPE model. Factors operative at the radar measurement scale present high potential to condition the distribution: DSD, vertical heterogeneity of reflectivity, beam blockage, distance from the radar, height of the beam, etc. A radar quality index (RQI) is produced in MRMS to represent the radar QPE uncertainty associated with beam blocking, reflectivity changes with height and near the melting layer [*Zhang et al.*, 2011b]. The information could be useful for segregating the uncertainty features in the Intermountain West where the radar sampling deficiencies impact the QPE. Another critical aspect to address in future work is the space-time correlation of the distributions. Evaluating the temporal and spatial correlation of the uncertainty structure is needed for application of the PQPE model to generate precipitation ensembles and investigate uncertainty propagation in hydrological

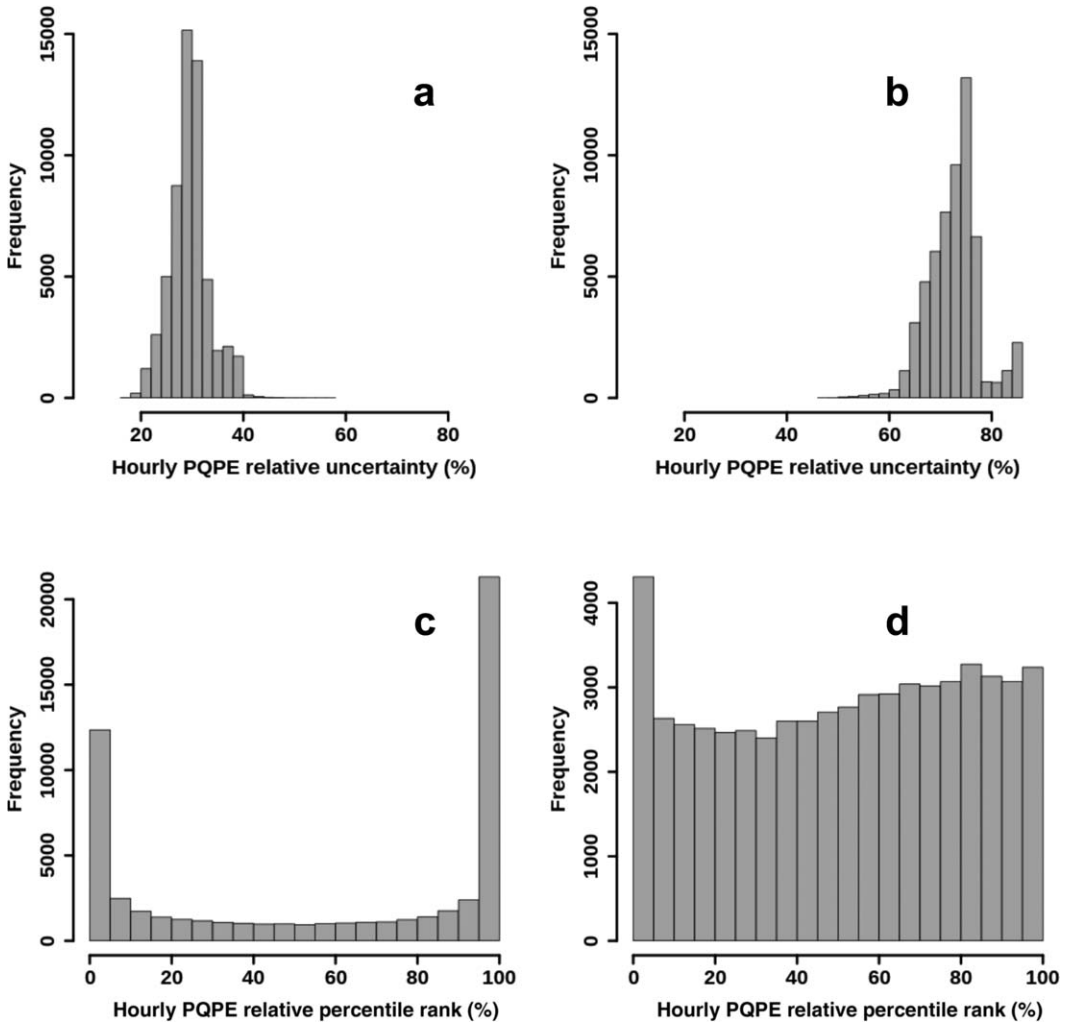

Figure 12. Distribution of the relative uncertainty of the hourly PQPE estimates with assuming (a) no correlation and (b) total correlation between 5 min PDFs; rank histogram of the hourly reference with respect to the ensemble QPE with assuming (c) no correlation and (d) total correlation between 5 min PDFs.

modeling. The correlation will be considered as a function of precipitation type and location in storm system.

The formulation of this model is general enough that it can be used for any other radar precipitation products [*Delrieu et al*., 2009; *Tabary*, 2007; *Zhang et al*., 2011a], including the polarimetric-based estimates [e.g., *Zrnic and Ryzhkov*, 1999; *Ryzhkov et al*., 2005]. Since it is based on radar observations and classification abilities, the PQPE framework is particularly suited for dual-polarized measurements. In the context of upgrades of the NEXRAD network to the dual-polarization technology and of MRMS, future work will address the expansion of the model to accommodate hydrometeor classification results and dual-pol moments such as the differential reflectivity, specific different phase, and specific attenuation.

The developed PQPE method will be applied for SWE, a research area in MRMS that is currently under way. Quantifying biases and uncertainties will be essential for SWE for applications such as road hazards during winter storms and water resources studies for basins that have snowpack. Physical parameters such as snow density and temperature need to be accounted for to improve SWE by active remote sensing. Beyond the characterization, the question of how to efficiently communicate probabilistic information to end-users is still outstanding. In order to evaluate how to communicate uncertainty information in the context of flash floods, forecasters at NCEP's Weather Prediction Center were involved in the interpretation of PQPE products that were generated in real time during the Flash Flood and Intense Rainfall (FFaIR) experiment during

the summer of 2013 [*Kirstetter et al*., 2013a]. User feedback will be instrumental in refining the use of QPE uncertainty relative to precipitation return periods in the context of flash flood forecasting. These PQPE products were further evaluated using forecaster feedbacks in the summer of 2014 during the Hazardous Weather Testbed experiment in Norman, OK.

Finally, this framework has great potential applications for satellite precipitation estimation and evaluation. *Kirstetter et al*. [2012, 2013b, 2014] characterized the variability of reference precipitation derived from MRMS and its impact when comparing with satellite precipitation estimates. In support of the Global Precipitation Measurement (GPM) mission, MRMS is used by a number of NASA investigators to evaluate level 2 and level 3 satellite precipitation algorithms. The PQPE methodology can reduce biases and will provide an improved characterization of the reference precipitation by considering the entire precipitation distribution. Future work will apply this framework to the Tropical Rainfall Measuring Mission (TRMM) Precipitation Radar in order to diagnose the *Z-R* relationships applied in the 2A25 algorithm, as well as to the dual-frequency precipitation radar onboard the core satellite of the GPM mission. Ultimately, we will promote the framework of PQPE to be applied to ground radar networks and also to space-based platforms.

Acknowledgments

We are very much indebted to the team responsible for the MRMS products who provided the data for this study. P.-E. Kirstetter was funded by a postdoctoral grant from the NASA Global Precipitation Measurement mission Ground Validation Management. Partial funding was provided by the NOAA/Office of Oceanic and Atmospheric Research under NOAA–University of Oklahoma Cooperative Agreement NA17RJ1227 to support Langston and Arthur. The authors would like to thank the three anonymous reviewers whose comments helped to improve the presentation significantly. The authors would like to thank Stasinopoulos, Rigby, Akantziliotou, and Ruckdeschel for making the gamlss [*Stasinopoulos and Rigby*, 2007] and distr [*Ruckdeschel et al*., 2006] freely available in R [*R Development Core Team*, 2012].

References

AghaKouchak, A., E. Habib, and A. Bárdossy (2010), Modeling radar rainfall estimation uncertainties: Random error model, *J. Hydrol. Eng.*, *15*(4), 265–274.

Berenguer, M., and I. Zawadzki (2008), A study of the error covariance matrix of radar rainfall estimates in stratiform rain, *Weather Forecast.*, *23*(6), 1085–1101.

Berne, A., and W. F. Krajewski (2013), Radar for hydrology: Unfulfilled promise or unrecognized potential?, *Adv. Water Resour.*, *51*, 357–366.

Chen, S., J. J. Gourley, Y. Hong, P. E. Kirstetter, J. Zhang, K. Howard, Z. Flamig, J. Hu, and Y. Qi (2013), Evaluation and uncertainty estimation of NOAA/NSSL next generation national mosaic QPE (Q2) over the Continental United States, *J. Hydrometeorol.*, *14*, 1308–1322.

Ciach, G. J. (2003), Local random errors in tipping-bucket rain gauge measurements, *J. Atmos. Oceanic Technol.*, *20*(5), 752–759.

Ciach, G. J., and W. F. Krajewski (1999), On the estimation of rainfall error variance, *Adv. Water Resour.*, *2*, 585–595.

Ciach, G. J., W. F. Krajewski, and G. Villarini (2007), Product-error-driven uncertainty model for probabilistic quantitative precipitation estimation with NEXRAD data, *J. Hydrometeorol.*, *8*, 1325–1347.

Creutin, J. D., and M. Borga (2003), Radar hydrology modifies the monitoring of flash flood hazard, *Hydrol. Processes*, *17*(7), 1453–1456.

Creutin, J. D., H. Andrieu, and D. Faure (1997), Use of weather radar for the hydrology of a mountainous area. Part II: Radar measurement validation, *J. Hydrol.*, *193*(1–4), 26–44.

Delrieu, G., B. Boudevillain, J. Nicol, B. Chapon, P. E. Kirstetter, H. Andrieu, and D. Faure (2009), Bollène-2002 experiment: Radar quantitative precipitation estimation in the Cévennes–Vivarais region, France, *J. Appl. Meteorol. Climatol.*, *48*, 1422–1447.

Delrieu, G., A. Wijbrans, B. Boudevillain, D. Faure, L. Bonnifait, and P.E. Kirstetter (2014), Geostatistical radar-raingauge merging: A novel method for the quantification of the rain estimation accuracy, *Adv. Water Resour.*, *71*, 110–124. doi:10.1016/j.advwatres.2014.06.005.

Germann, U., M. Berenguer, D. Sempere-Torres, and M. Zappa (2009), Real-ensemble radar precipitation estimation for hydrology in a mountainous region, *Q. J. R. Meteorol. Soc.*, *135*(639), 445–456.

Gourley, J. J., B. Kaney, and R. A. Maddox (2003), Evaluating the calibrations of radars: A software approach, in *Thirty-First International Conference on Radar Meteorology*, pp. 459–462, Am. Meteorol. Soc., Seattle, Wash. [Available at https://ams.confex.com/ams/32BC31R5C/techprogram/paper_64171.htm.]

Habib, E., and L. Qin (2013), Application of a radar-rainfall uncertainty model to the NWS multi-sensor precipitation estimator products, *Meteorol. Appl.*, *20*, 276–286.

Habib, E., G. J. Ciach, and W. F. Krajewski (2004), A method to filtering out raingauge representativeness errors from the verification distributions of radar and raingauge rainfall, *Adv. Water Resour.*, *27*, 967–980.

Habib, E., A. V. Aduvala, and E. A. Meselhe (2008), Analysis of radar–rainfall error characteristics and implications for streamflow simulation uncertainty, *Hydrol. Sci. J.*, *53*(3), 568–587.

Hou, A. Y., R. K. Kakar, S. Neeck, A. A. Azarbarzin, C. D. Kummerow, M. Kojima, R. Oki, K. Nakamura, and T. Iguchi (2014), The global precipitation measurement (GPM) mission, *Bull. Am. Meteorol. Soc.*, *95*, 701–722, doi:http://dx.doi.org/10.1175/B.

Jordan, P. W., A. Seed, and P. E. Weinmann (2003), A stochastic model of radar measurement errors in rainfall accumulations at catchment scale, *J. Hydrometeorol.*, *4*(5), 841–855.

Kirstetter, P. E., G. Delrieu, B. Boudevillain, and C. Obled (2010), Toward an error model for radar quantitative precipitation estimation in the Cévennes-Vivarais region, *France, J. Hydrol.*, *394*(1–2), 28–41.

Kirstetter, P. E., Y. Hong, J. J. Gourley, S. Chen, Z. Flamig, J. Zhang, M. Schwaller, W. Petersen, and E. Amitai (2012), Toward a framework for systematic error modeling of spaceborne precipitation radar with NOAA/NSSL ground radar-based national mosaic QPE, , *J. Hydrometeorol.*, *13*(4), 1285–1300.

Kirstetter, P. E., J. J. Gourley, Y. Hong, S. Moazamigoodarzi, and E. Mintmire (2013a), Probabilistic quantitative precipitation estimates with NOAA/NSSL ground radar-based national mosaic and QPE system, in *36th Conference on Radar Meteorology*, Am. Meteorol. Soc., Breckenridge, Colo. [Available at https://ams.confex.com/ams/36Radar/webprogram/Paper228901.html.]

Kirstetter, P. E., N. Viltard, and M. Gosset (2013b), An error model for instantaneous satellite rainfall estimates: Evaluation of BRAIN-TMI over West Africa, *Q. J. R. Meteorol. Soc.*, *139*, 894–911.

Kirstetter, P. E., Y. Hong, J. J. Gourley, Q. Cao, M. Schwaller, and W. Petersen (2014), Research framework to bridge from the global precipitation measurement mission core satellite to the constellation sensors using ground-radar-based national Mosaic QPE, chap. 4, in *Remote Sensing of the Terrestrial Water Cycle*, edited by V. Lakshmi et al., John Wiley, Hoboken, N. J. doi:10.1002/9781118872086.

Krajewski, W. F., and K. P. Georgakakos (1985), Synthesis of radar rainfall data, *Water Resour. Res.*, *21*, 764–768.

Krajewski, W. F., and J. A. Smith (2002), Radar hydrology: Rainfall estimation, *Adv. Water Resour.*, *25*(8–12), 1387–1394.

Lakshmanan, V., A. Fritz, T. Smith, K. Hondl, and G. Stumpf (2007), An automated technique to quality control radar reflectivity data, *J. Appl. Meteorol. Climatol.*, *46*, 288–305.

Mandapaka, P. V., and U. Germann (2010), Radar-rainfall error models and ensemble generators, in *Rainfall: State of the Science, AGU Geophys. Monogr. Ser.*, vol. 191, edited by F. Y. Testik and M. Gebremichael, pp. 247–264, AGU, Washington, D. C.

Rigby, R. A., and D. M. Stasinopoulos (2005), Generalized additive models for location, scale and shape, *J. R. Stat. Soc. Ser. C Appl. Stat.*, *54*, 507–554.

R Core Team (2012), R: A Language and Environment for Statistical Computing, R Found. for Stat. Comput., Vienna, Austria. ISBN 3-900051-07-0. [Available at http://www.R-project.org/.]

Ruckdeschel, P., M. Kohl, T. Stabla, and F. Camphausen (2006), S4 classes for distributions, *R News*, *6*(2), 2–6.

Ryzhkov, A. V., T. J. Schuur, D. W. Burgess, P. L. Heinselman, S. E. Giangrande, and D. S. Zrnic (2005), The joint polarization experiment, polarimetric rainfall measurements and hydrometeor classification, *Bull. Am. Meteorol. Soc.*, *86*(6), 809–824.

Simanton, J. R., and H. B. Osborn (1980), Reciprocal distance estimate of point rainfall, *J. Hydraul. Div. Am. Soc. Civ. Eng.*, *106*, 1242–1246.

Stasinopoulos, D. M., and R. A. Rigby (2007), Generalized additive models for location scale and shape (GAMLSS) in R, *J. Stat. Software*, *10*, 1–46.

Tabary, P. (2007), The new French operational radar rainfall product. Part 1: Methodology, *Weather Forecast.*, *22*(3), 393–408.

Tian, Y., G. J. Huffman, R. F. Adler, L. Tang, M. Sapiano, V. Maggioni, and H. Wu (2013), Modeling errors in daily precipitation measurements: Additive or multiplicative?, *Geophys. Res. Lett.*, *40*, 2060–2065, doi:10.1002/grl.50320.

Vasiloff, S., et al. (2007), Improving QPE and very short term QPF: An initiative for a community-wide integrated approach, *Bull. Am. Meteorol. Soc.*, *88*, 1899–1911.

Villarini, G., W. F. Krajewski, G. J. Ciach, and D. L. Zimmerman (2009), Product-error-driven generator of probable rainfall conditioned on WSR-88D precipitation estimates, *Water Resour. Res.*, *45*, W01404, doi:10.1029/2008WR006946.

Villarini, G., B. C. Seo, F. Serinaldi, and W. F. Krajewski (2013), Spatial and temporal modeling of radar rainfall uncertainties, *Atmos. Res.*, *135–136*, 91–101.

Xu, X., K. Howard, and J. Zhang (2008), An automated radar technique for the identification of tropical precipitation, *J. Hydrometeorol.*, *9*, 885–902.

Zawadzki, I. (1982), The quantitative interpretation of weather radar measurements, *Atmos. Ocean*, *20*(2), 158–180.

Zhang, J., K. Howard, and J. J. Gourley (2005), Constructing three-dimensional multiple radar reflectivity mosaics: Examples of convective storms and stratiform rain echoes, *J. Atmos. Oceanic Technol.*, *22*, 30–42.

Zhang, J., et al. (2011a), National mosaic and multi-sensor QPE (NMQ) system: Description, results, and future plans, *Bull. Am. Meteorol. Soc.*, *92*, 1321–1338.

Zhang, J., Y. Qi, K. Howard, C. Langston, and B. Kaney (2011b), Radar quality index (RQI)—A combined measure of beam blockage and VPR effects in a national network, in *Proceedings of International Symposium on Weather Radar and Hydrology*, vol. *351*, pp. 388–393, IAHS Publ. [Available at https://www.nssl.noaa.gov/projects/q2/tutorial/images/mosaic/WRaH_Proceedings_Zhang-et-al_v3.pdf.]

Zrnic, D. S., and A. V. Ryzhkov (1999), Polarimetry for weather surveillance radar, *Bull. Am. Meteorol. Soc.*, *80*, 389–406.